Substitution of metallocene with [2.2]-paracyclophane to enable confocal microscopy imaging in living cells

Joanna Skiba,[a] Claudia Schmidt,[b] Petra Lippmann,[b] Philipp Ensslen,[c] Hans-Achim Wagenknecht,[c] Rafał Czerwieniec,*[d] Fabian Brandl,[d] Ingo Ott,[b] Tytus Bernaś,[e] Barbara Krawczyk,[f] Dominik Szczukocki,[f] Konrad Kowalski,*[a]

[a]J. Skiba, K. Kowalski Faculty of Chemistry, Department of Organic Chemistry University of Łódź Tamka 12, PL-91403 Łódź, Poland
[b]C. Schmidt, P. Lippmann, I. Ott Institute of Medicinal and Pharmaceutical Chemistry Technische Universität Braunschweig Beethovenstr. 55, D-38106 Braunschweig, Germany
[c]P. Ensslen, H.-A. Wagenknecht Institute of Organic Chemistry Karlsruhe Institute of Technology Fritz-Haber-Weg 6, 76131 Karlsruhe, Germany
[d]R. Czerwieniec, F. Brandl Institut für Physikalische und Theoretische Chemie Universität Regensburg Universitätsstraße 31, D-93040 Regensburg, Germany
[e]T. Bernaś Nencki Institute of Experimental Biology Polish Academy of Sciences ul. Pasteura 3, 02-093 Warsaw, Poland
[f]B. Krawczyk, D. Szczukocki Faculty of Chemistry, Department of Inorganic and Analytical Chemistry University of Łódź Tamka 12, PL-91403 Łódź, Poland

Eur. J. Inorg. Chem. 2017, 297–305
DOI: 10.1002/ejic.201600281

This project has received funding from the European Union's Horizon 2020 research and innovation programme under the Marie Skłodowska-Curie grant agreement No. 645628

Project Number: 645628
Project Acronym: METCOPH
Project title: Metallocomplexes of macrocyclic compounds for photonic devices

Substitution of metallocene with [2.2]-paracyclophane to enable confocal microscopy imaging in living cells

Joanna Skiba,[a] Claudia Schmidt,[b] Petra Lippmann,[b] Philipp Ensslen,[c] Hans-Achim Wagenknecht,[c] Rafał Czerwieniec,*[d] Fabian Brandl,[d] Ingo Ott,[b] Tytus Bernaś,[e] Barbara Krawczyk,[f] Dominik Szczukocki,[f] Konrad Kowalski,*[a]

Abstract: Bioimaging techniques allowing for visualization of ferrocene in living cells do not exist.This work addresses this challenging problem, and a new non-direct approach for the bioimaging of ferrocenyl compounds in living and fixed cells is proposed. It is based on the structural similarity of metallocenyl (ferrocenyl and ruthenocenyl) groups to their metal-free [2.2]-paracyclophanyl congeners. Three adequately designed compounds were obtained. They share a 5-(1-ethynylpyrenyl)-uracil group as a common structural motif and differ in their three-dimensional aromatic substituents: [2.2]-paracyclophanyl, ferrocenyl or ruthenocenyl. The first substituent allows for pyrenyl luminescence to occur, while the latter two act as quenchers. The accumulation of the luminescent derivative in the membranes, cytoplasm and mitochondria of living and fixed cells was confirmed by confocal microscopy. Microscopy studies were further correlated with HR-CS AAS measurements of the ruthenocenyl compound that confirmed the uptake of ruthenium into the cells. Thus, taking into account the overall similarity of the compounds under study, it can be hypothesized that metallocenyl derivatives are localized in the membranes, cytoplasm and mitochondria of assayed cells. This is a basis for the more general concept of the utilization of luminescent [2.2]-paracyclophanes as probes in non-direct bioimaging studies of metallocene derivatives.

[a] J. Skiba, K. Kowalski
Faculty of Chemistry, Department of Organic Chemistry
University of Łódź
Tamka 12, PL-91403 Łódź, Poland
E-mail: kondor15@wp.pl (Konrad Kowalski)
[b] C. Schmidt, P. Lippmann, I. Ott
Institute of Medicinal and Pharmaceutical Chemistry
Technische Universität Braunschweig
Beethovenstr. 55, D-38106 Braunschweig, Germany
[c] P. Ensslen, H.-A. Wagenknecht
Institute of Organic Chemistry
Karlsruhe Institute of Technology
Fritz-Haber-Weg 6, 76131 Karlsruhe, Germany
[d] R. Czerwieniec, F. Brandl
Institut für Physikalische und Theoretische Chemie
Universität Regensburg
Universitätsstraße 31, D-93040 Regensburg, Germany
[e] T. Bernaś
Nencki Institute of Experimental Biology
Polish Academy of Sciences
ul. Pasteura 3, 02-093 Warsaw, Poland
[f] B. Krawczyk, D. Szczukocki
Faculty of Chemistry, Department of Inorganic and Analytical Chemistry
University of Łódź
Tamka 12, PL-91403 Łódź, Poland

Supporting information for this article is given via a link at the end of the document.((Please delete this text if not appropriate))

Introduction

The importance of metal complexes in biological and medicinal applications is steadily increasing. Without any doubt, this is at least in part due to the development of Pt-based anticancer agents, which have been successfully introduced into clinical practice during the last several decades.[1] In addition to inorganic complexes, organometallic compounds (comprising one or more metal-carbon bonds) have also become increasingly important in biology and medicine.[2] Within this structurally rich and diverse class of compounds, ferrocenyl derivatives have been the focus of research as potential anticancer,[3] antibacterial[2f] and antiparasitic drugs.[4] Ferrocene (FcH) (Fig. 1) itself is an aromatic compound with a unique three-dimensional (3D) sandwich-like molecular structure, reversible electrochemistry, and well-developed methods of derivatization.[2h,5] For these combined structural, physico-chemical, and chemical reasons, ferrocenyl derivatives have been extensively studied for the above-mentioned biomedical applications.

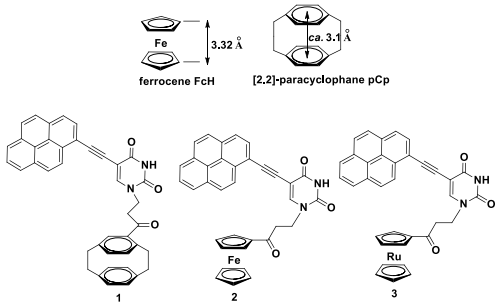

Figure 1. Structures of ferrocene FcH, [2.2]-paracyclophane pCp, and aryl-uracil-pyrenes **1-3** studied in this work.

However, the detailed mechanisms of the biological action of ferrocenes are understood only for some classes of these molecules.[3b] To determine which biological structures (cells, cellular compartments) and macromolecules are affected, it is necessary to obtain information about the fate of a given ferrocene derivative upon application to the biological target. It is necessary to know where it accumulates, how fast it is transported and for how long it remains stable. Thus, the challenging questions about the mechanisms of biological action

must be discussed in the broader context of the bioimaging of organometallic compounds.

For bioimaging studies, fluorescence confocal microscopy techniques are particularly appealing.[6] However, their applicability is restricted to luminescent materials. Organometallic compounds lacking luminophore groups or compounds whose emission is quenched in the studied environment cannot be detected. Unfortunately, such non-emissive compounds represent the majority of bio-relevant organometallic complexes.

For the bioimaging of non-luminescent complexes, other techniques such as atomic absorption spectroscopy (AAS),[7] inductively coupled plasma mass spectroscopy (ICP-MS),[8] and X-ray fluorescence microscopy (XRF),[9] can be used. AAS is an excellent technique that offers high sensitivity, but it requires biological sample destruction prior to measurement. ICP-MS is more sensitive than AAS, but access to this relatively new analytical technique is still quite limited. The use of XRF is also restricted because it requires access to a synchrotron along with specialized equipment. Furthermore, this technique causes damage to biological samples. All three of these techniques allow for quantitative and qualitative measurements of metal contents in biological samples, but they do not provide information on the ligands surrounding the metallic centre. They also cannot be used for uptake studies when metals with high intrinsic cellular levels (*e.g.,* Fe) are involved.

Metal-carbonyl complexes, due to their strong absorption bands corresponding to the ν(CO) modes in the IR region (1800-2200 cm^{-1}), a region that is generally free from the absorbance of biomolecules, can conceivably be bioimaged inside cells or tissues with vibrational spectroscopy detection techniques.[10] When the metal-carbonyl unit is attached to the proper ligand, dual-modality (IR and luminescent) techniques can be used for bioimaging studies.[11]

However, none of the above techniques can be successfully applied for the bioimaging of ferrocene derivatives in living or fixed cells or tissues. This is because ferrocenes are not luminescent, and iron is a naturally abundant element. In addition, the ferrocenyl group does not exhibit characteristic IR absorption bands discernible from the IR absorption of common biomolecules. Literature survey shows two reports focused on cellular bioimaging with ferrocenes. In both approaches, non-direct imaging methods were applied: (i) nano-imaging of a rutenocenyl analog of ferroquine in parasitic digestive vacuoles with a XRF technique[4c] and (ii) fluorescence detection of an anthryl group liberated from a non-emissive anthracene-ferrocene conjugate in HeLa cells.[6f]

In this contribution, we report *in vitro* cellular confocal microscopy bioimaging studies of luminescent [2.2]-paracyclophane derivative **1** as a structural analogue of non-luminescent ferrocenyl and ruthenocenyl derivatives **2** and **3**, respectively (Fig. 1). Apparently, the structural similarity of [2.2]-paracyclophane (pCp) (Fig. 1) and ferrocene allows for the use of the former as a metal-free analogue of the latter. In fact, ferrocene[5] and [2.2]-paracyclophane (pCp)[12] can be regarded as “tween” molecules. They both exhibit aromatic character and have a similar size and external shape of their 3D structures, which are sandwich-like (FcH) and layered (pCp),[13] respectively. In the [2.2]-paracyclophane molecule, the two benzene rings are bound at their 1,4-positions by CH_2CH_2 linkers, which forces them to accommodate a boat-like conformation. The distance between the bottoms of the boat-like rings is ca. 3.1 Å. A similar value of 3.32 Å was measured for the distance between the two cyclopentadienyl rings in ferrocene. Moreover, ferrocene and [2.2]-paracyclophane show similar reactivity behaviour (*e.g.,* both undergo Friedel-Crafts-type reactions) and exhibit a similar lipophilic character.[14] Next to numerous above mentioned similarities between pCp and FcH, these molecules differ in respect to electrochemical behaviour. Cyclovoltametric oxidation waves of pCp display irreversible character,[12d] while one-electron oxidation of FcH is reversible.[5i]

The above-mentioned structural similarities between FcH and pCp rationalize the question whether these compounds can interact with the same biological target when functionalized by the same or similar groups and substituents. To the best of our knowledge, this interesting problem has been addressed solely for some examples of ferrocenyl and [2.2]-paracyclophanyl dopamine receptor ligands.[15] Accordingly, it has been reported that ferrocenyl ligands display partial agonist properties, while their [2.2]-paracyclophane congeners exhibit neutral D3 antagonism.[15a] For the purpose of these studies, three closely related compounds **1-3** were designed and synthesized. They all feature a 5-(1-ethynylpyrenyl)-uracil group as a common structural motif. Metallocenes **2** and **3** are ferrocenyl-nucleobases, a group of bioconjugates with increasing importance in medicinal chemistry.[16]

The presence of the pyrenyl group is crucial in our design due to the luminescent properties of this group.[17] These properties are not observed in combination with metal-containing ferrocenyl and ruthenocenyl groups, which effectively quench the emission. However, the replacement of the metallocene group with a purely organic [2.2]-paracyclophanyl group renders compound **1** a strongly emissive analogue of complexes **2** and **3**. Thus, compound **1** can serve as a fluorescent probe, and its bio-distribution in living cells can be assessed with confocal microscopy. Keeping in mind the above-discussed structural similarity of ferrocene and [2.2]-paracyclophane scaffolds, the cellular bio-distribution of **1** was investigated by means of confocal microscopy in living and fixed cells. The knowledge acquired from these experiments can then be applied to its non-emissive congeners **2** and **3**. The cellular uptake of the ruthenium compound **3** was measured using high-resolution continuum-source atomic absorption spectroscopy (HR-CS AAS).[18] With this method, ruthenium from the ruthenocene complex **3** can be quantified. Prior to the confocal microscopy studies, compound **1** was subjected to TD-DFT computations and detailed spectroscopic characterization. In this paper, we also report on the interactions of **1** with the $(dA)_{20}$ oligonucleotide.

Results and Discussion

Synthesis and Characterization

The compounds **1**, **2**, and **3** were obtained in 52%, 56%, and 55% yields, respectively, via the Sonogashira cross-coupling

reaction of 5-iodouracil derivatives **4**, **5,** and **6** and 1-ethynylpyrene (Scheme 1).

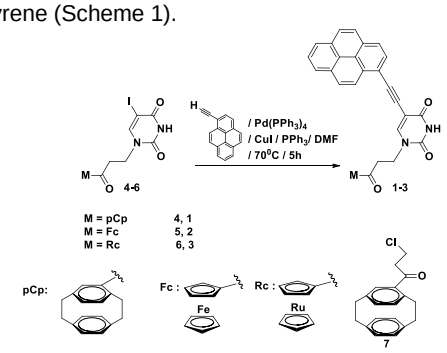

Scheme 1. Pd-catalysed synthesis of compounds **1-3**.

The syntheses of substrates **5** and **6** were recently described.[16b] To prepare the starting **4**, a two-step synthetic approach was applied. In the first step, a Friedel-Crafts reaction of [2.2]-paracyclophane and 3-chloropropionyl chloride afforded racemic 3-chloropropionyl-[2.2]-paracyclophane **7** in 53% yield (Scheme S1). In the second step, the reaction of **7** with 5-iodouracil under literature conditions[16b] afforded product **4** in 76% yield (Scheme S2). Compounds **1** and **3** are yellow air-stable solids, whereas compound **2** is an orange-red air-stable solid. All newly obtained compounds were characterized by standard spectroscopic methods, including ^{1}H-NMR, ^{13}C-NMR, and IR spectroscopy, MS, and elemental analysis. All analytical data confirm their proposed structures. The ^{1}H-NMR spectra of compounds **1**-**3** are presented in Figures S1-S5. The stability of compounds **1**-**3** was examined in aerated DMSO-d_6 solution by ^{1}H-NMR spectroscopy. No signs of decomposition were observed after 72 h for any of the tested compounds. Relevant ^{1}H-NMR spectra are presented in Figures S6-S8 (*Supplementary Information)*.

Photophysical properties of compound 1.

The near-UV part of the absorption spectrum of compound **1** is dominated by a strong structured band with maxima at 393 and 370 nm, as measured in ethanol at ambient temperature. (Fig. 2) With the molar absorption coefficient ε(393 nm) of $3.9 \cdot 10^5$ mol^{-1} cm^{-1} dm^3 the corresponding transition is strongly allowed, which points to its π-π* character. The spectrum of **1** closely resembles the absorption spectra of other 1-pyrene derivatives with π-conjugated substituents, e.g., 1-phenylethynylpyrene.[19] Thus, in analogy to the literature, the lowest absorption band is assigned to a “pyrene-like” transition, similar to the strongly allowed $S_2 \leftarrow S_0$ transition in unsubstituted pyrene. This assignment is further supported by the results of TD-DFT calculations. Both the HOMO and LUMO in **1** (Fig. 3) are derived from the HOMO and LUMO of pyrene, with significant contributions from the uracilethynyl group. The elongation of the aromatic system raises the HOMO (π orbital) energy and lowers the LUMO (π* orbital) energy, leading to a substantial red shift of the HOMO – LUMO transition as compared to pyrene, in which a similar HOMO – LUMO excitation gives rise to a band ($S_2 \leftarrow S_0$) at 334 nm.[19] Information concerning the higher excited states of **1** is given in the *Supplementary Information*.

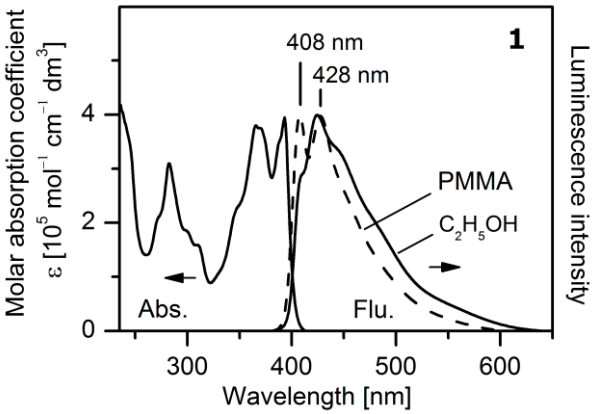

Figure 2. Ambient temperature UV-Vis absorption spectrum of **1** in ethanol and luminescence spectra of **1** recorded in poly(methyl methacrylate) (PMMA) and ethanol upon excitation at λ_{exc} = 360 nm at ambient temperature. At 408 and 428 nm, two apparent maxima due to the partly resolved vibronic structure of the emission spectrum in PMMA are indicated.

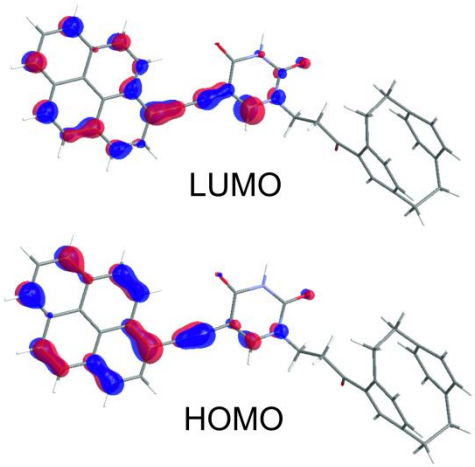

Figure 3. Kohn-Sham frontier molecular orbitals in compound **1**.

Compound **1** is strongly luminescent both in diluted solution and in a polymer film. The respective emission spectra recorded at ambient temperature in ethanol and poly(methyl methacrylate) (PMMA) are reproduced in Fig. 2. The spectrum measured in PMMA displays a partly resolved vibronic structure resembling the shape of the lowest absorption band (mirror image). The two spectra intersect at 400 nm (25 000 cm^{-1}), indicating that the same transition($S_1 \leftrightarrow S_0$; $E(S_1) \approx 25\,000$ cm^{-1}), is responsible for the both absorption and emission bands. The luminescence profile observed in solution deviates from that in a rigid polymer sample. In ethanol, higher-energy vibronic satelites gain intensity relative to the purely electronic origin. Thus, the observed intensity maximum is red-shifted to 424 nm (Table 1 and Fig. 2). Such solvent dependencies of the vibronic structure of the fluorescence spectra were observed for free pyrene in

different solvents and reflect specific interactions between the excited singlet state of pyrene with the solvent molecules, mostly related to the different dipole-dipole interactions.[20] Owing to the distinctly allowed character of the $S_1 \leftrightarrow S_0$ transition (oscillator strength $f = 0.96$; Table S1), compound **1** displays very short fluorescence lifetimes of 1.2 ns in PMMA and 0.5 ns in ethanol, with very high luminescence quantum yields of 53 and 44 %, respectively. (Table 1)

Table 1. Ambient temperature luminescence data for compound **1** in poly(methyl methacrylate) (PMMA) and in ethanol solution.

Solvent/ Matrix	Emission energy λ_{em}	Quantum yield ϕ_{em}	Decay time τ_{em}
PMMA	408 nm	53 %	1.2 ns
C_2H_5OH	424 nm[a]	44 %	0.5 ns

a) Emission maximum.

Interactions of 1 with oligonucleotide $(dA)_{20}$

We recently evidenced the self-assembly of ethynyl-pyrene- and ethynyl-Nile red-modified 2'-deoxyuridine nucleosides along a single stranded oligo-2'-deoxyadenosine as template.[17a,21] The self-assembly process is guided by the hydrogen-binding motif and driven by the π-π stacking between the chromophores. It is obvious that there is a similarity between the 5-(1-ethynylpyrenyl)-2'-deoxyuridine and compound **1**. According to the canonical base pairing, the uracil unit of compound **1** should offer a binding site to adenines as part of the DNA template. UV-Vis spectroscopy was used to investigate such behaviour of **1** (Fig. 4).

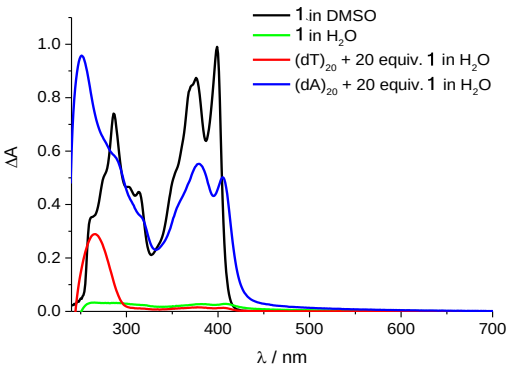

Figure 4. 25 µM **1** in DMSO (black), in water (green), 20 equiv. **1** with 2.5 µM $(dA)_{20}$ (blue) and 2.5 µM $(dT)_{20}$ (red) in water + 0.6 % DMSO.

Compound **1** is neither soluble in pure water nor in water with 0.6 % dimethylsulfoxid (DMSO) in the presence of the "wrong" template oligo-2'-deoxythymidine $(dT)_{20}$. In contrast, in the presence of the right (i.e., complementary) template oligo-2'-deoxyadenosine $(dA)_{20}$, **1** becomes soluble, which indicates selective binding to the DNA template (dA vs. dT). Compared to **1** in DMSO, the absorption of the ethynylpyrene chromophore of **1** is red-shifted, its extinction hypochromically shifted, and the ratio between the absorption maxima corresponding to the vibronic structure of the $S_1 \leftarrow S_0$ transition change from 1.13 in DMSO (black line in Fig. 4; the long-wavelength maximum shows larger extinction) to 0.91 in water containing $(dA)_{20}$ (blue line in Fig. 4; shorter-wavelength satelites gain relative intensity). Thus, these solubility and spectral changes indicate a successful arrangement of **1** along $(dA)_{20}$ acting as a specific DNA template. The emission of **1** in the presence of $(dA)_{20}$ additionally indicates the chromophore assembly (Fig. 5). In contrast to DMSO and ethanol solutions, showing blue fluorescence characteristic for (non-agregated) ethynyl pyrene, in aqueous $(dA)_{20}$ solution a broad green emission with a maximum at 505 nm is observed (Fig. 5). This behaviour is assigned to formation of pyrene excimers.[17d-g] Thus, occurrence of this broad green emission at the expense of the short-wavelength emission (displayed by **1** in a diluted ethanolic or DMSO solution) clearly indicates specific binding of molecules **1** to the $(dA)_{20}$ scaffold with ethynylpyrene groups of the thus formed aggregate being close one to each other. The spatial proximity of the ethynylpyrene groups leads to effective π-π interactions and thus, excimer formation upon excitation with light.

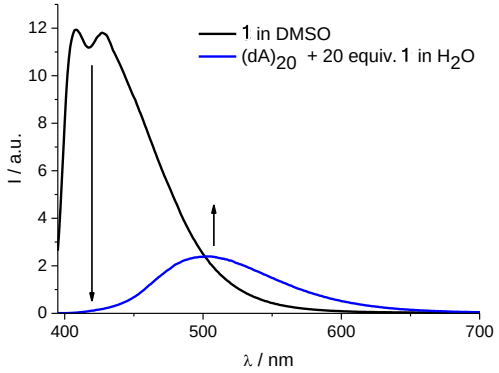

Figure 5. Emission spectra (λ_{exc} = 380 nm) of 25 µM **1** in DMSO (black) and 20 equiv. **1** with 2.5 µM $(dA)_{20}$ (blue) in water + 0.6 % DMSO.

Confocal Microscopy

The luminescence of **1** was used to study the uptake and distribution of this compound in live HeLa cells. A concentrated stock solution of **1** in dimethyl sulfoxide (DMSO) was diluted with cell culture medium (DMEM) in a 1:2000 volume ratio (0.1 µM). Thus, the amount of DMSO in the medium was below 0.1 %, which helped to mitigate the potential toxic effect of the solvent. The viability of the cells (measured with a propidium iodide/fluorescein acetate (PI/FDA) test) was greater than 98% following 4 hours of incubation with **1**. In a separate experiment, where no PI or FDA was present, the diffuse luminescence of **1** was detectable in the cell interiors (Fig. 6).

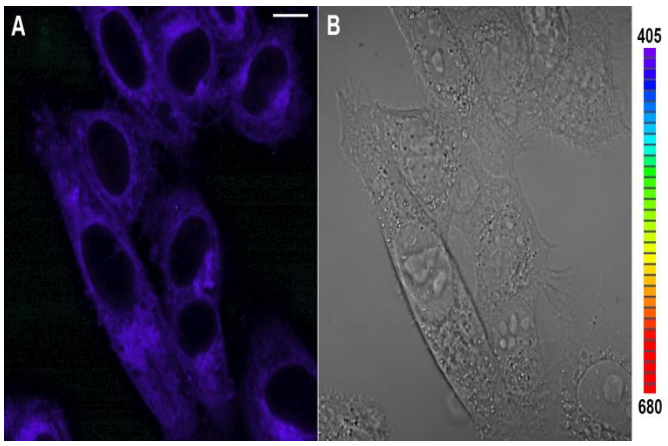

Figure 6. Luminescence of **1** (A) and transmitted light (B) image of living HeLa cells. The luminescence is represented in a false colour scale (right), with colours corresponding to spectral bands. Scale bar 10 µm.

This staining pattern became stable after 1 hour of incubation with **1**. The luminescence spectrum (λ_{exc} = 355 nm, Fig. 7) was compatible with the results obtained in solution (Figs. 2 and 5). However, following strong (10 s at 5 mW laser power) laser irradiation, the overall luminescence intensity decreased, and the emission spectrum red shifted to a maximum at ca. 500 nm. (Fig. 7).

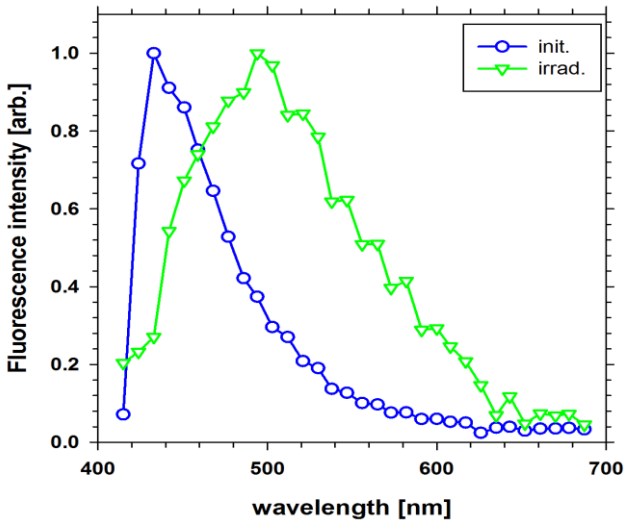

Figure 7. Emission spectra (λ_{exc} = 355 nm) of **1** in live HeLa cells before (blue) and after photoconversion (green).

The subcellular distribution was not affected by this photoconversion, however. The emission from the cell membranes and cytoplasm was detected but no luminescence stemming from the nuclei, as indicated by the comparison of the transmitted light and luminescence images (Fig. 6). A similar pattern was obtained in fixed HeLa cells (Fig. 8).

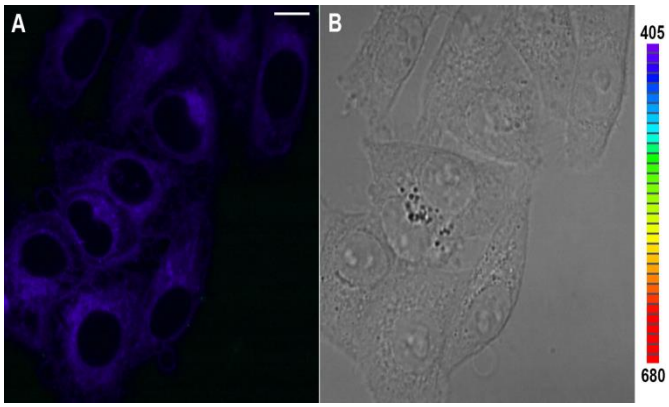

Figure 8. Luminescence of **1** (A) and transmitted light (B) image of fixed HeLa cells. The luminescence is represented in a false colour scale (right), with colours corresponding to spectral bands. Scale bar 10 µm.

This permitted us to use acridine orange (AO), which stains DNA in nuclei (green fluorescence) and RNA in the cytoplasm (red luminescence). The comparison of the subcellular distributions of **1** and AO (Fig. 9 and Fig. S11) confirms the exclusion of the former from the nuclei.

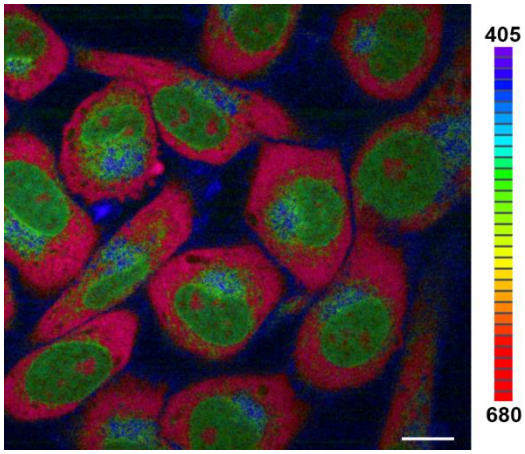

Figure 9. Subcellular distributions of DNA in nuclei (AO, green), RNA in cytoplasm (AO, red), and regions corresponding to elevated luminescence of **1** (blue) in fixed HeLa cells. Scale bar 10 µm.

The distribution of cytoplasmic **1** is not uniform, and this effect might originate from mitochondrial staining. This is compatible with the fact that the accumulation of **1** in the interiors of the HeLa cells was disrupted by potential sensitive mitochondrial probes (TMRE and JC-1, data not shown).
In the next stage, the luminescence decay was measured, on cell by cell basis in HeLa cells. The decays are distinctly non-monoexponential, probably due to significant inhomogeneity of the local environments in the biological membranes, but the decay profiles are uniform for all different cell regions investigated. A fit of a tri-exponential decay function to the measured decay curve reveals three time constants of 0.8 ns, 2.4 ns, and 9.1 ns, giving an average lifetime (intensity

weighted) of 4.9 ± 0.4 (Fig.S13A). The cells stained with **1** were then imaged in the presence of the ferrocenyl derivative **2** used at a five-fold concentration of compound **1**. After 10 minutes of incubation, an increase of the luminescence lifetime of **1** was observed (Fig.S13B) to 5.5 ± 0.3 ns. One may note that no changes of subcellular distribution of **1** luminescence but its average intensity increased by a factor of 1.4. Likewise, the component times of the luminescence decay model were similar in the presence and in the absence of **2**. Thus, the increase of the emission lifetime corresponded to an increase of the contribution of the longest decay component. The above co-staining experiment seems to supports the idea that molecules of **1** and **2** are co-localised in the same compartments of the living cell. One can hypothesise that complex **2** alternates the self-assembly of **1** in a quasi-crystal lipid bilayers to form aggregates or/and dimers.

Cytotoxicity and cellular ruthenium uptake

The antiproliferative effects of compounds **1**- **3** were determined in two cancer cell lines, namely, human HT-29 colon carcinoma cells and oestrogen receptor negative MDA-MB-231 mammary carcinoma cells. However, for none of the compounds could an IC_{50} value be obtained, even at the highest investigated concentration of 100 µM. Whereas these results prevent the application of **1**- **3** as anticancer agents, for compound **1**, the absent cell toxicity corroborates its use as a luminescent probe in the bioimaging of live cells.
Next, the ruthenium levels in HT-29 cells exposed for 1 h or 6 h to 5.0 µM **3** were measured by high-resolution continuum source atomic absorption spectrometry (HR-CS AAS). The results are expressed as nmol of compound per milligram of total cell protein and afforded a cellular level of 0.96 (±0.35) nmol/mg after 1 hour. The cellular uptake of compound **3** increased over time, and the complex reached a cellular level of 4.72 (±0.17) nmol / mg after 6 h.

Determination of log $P_{o/w}$

The octanol/water partition coefficient log $P_{o/w}$ is an important parameter for the investigation of the fate of organic compounds and drugs in organs and tissues. Herein, to determine the log $P_{o/w}$, a chromatographic method was used.[22] Lipophilicity estimation using RP-HPLC is based on the principle of the partition of a solute between a high-polarity eluent and a low-polarity stationary phase. The values of log $P_{o/w}$ for compounds **1-3** were evaluated by the extrapolation of the experimental relationships between the logarithm of the solute retention and the organic modifier concentration in the aqueous effluent. For the extrapolation, the Soczewiński-Wachtmeister relationship[22d] was applied. For all tested compounds, good linear correlations with high coefficients of determination (R^2) were achieved (Table 2 and *Supplementary Information*).

Table 2. Equations and values of R^2 coefficient and log $P_{o/w}$ for the studied compounds.

compound	equation	R^2	log $P_{o/w}$
1	y = -0.0702x + 6.9788	0.9978	6.9
2	y = -0.0577x + 5.4806	0.9971	5.4
3	y = -0.0581x + 5.4711	0.9975	5.4

The studied compounds display log $P_{o/w}$ values in the range of 5.4 to 6.9. Thus, they are distinctly lipophilic and exhibit a high affinity to lipid-rich cellular compartments.[23] Hence, all three compounds under study are expected to accumulate in lipid membranes and lipid cytoplasmic compartments more than in other cellular structures. Indeed, this assumption is confirmed by confocal microscopy studies with the luminescent compound **1** (see Confocal Microscopy section above.) From the three compounds studied in this work, the [2,2]-paracyclophane derivative **1** with log $P_{o/w}$ = 6.9 displays the most lipophilic character, followed by the ruthenocene and ferrocene derivatives **3** and **2** with log $P_{o/w}$ = 5.4. Thus, differences in lipophilicity related to the different polarity of the paracyclophanyl and metallocenyl groups are evident. Differences of log $P_{o/w}$ of 1.5, as displayed by compounds **1**-**3** can be biologically manifested by different kinetics of accumulation in lipid cellular compartments. However, since the log $P_{o/w}$ values for all three compounds point to a definitely lipophilic character, such differences, are not expected to alter cellular accumulation pattern itself.

Conclusions

In summary, the synthesis of three structurally closely related 3D aromatic systems bearing a common uracil-ethynylpyrenyl substituent is reported. The pyrenyl group acts as a luminescent reporter entity enabling the detection of the [2.2]-paracyclophane derivative **1** in living as well as in fixed cells. The emission of compound **1** is characterized by a high quantum yield of up to 53%. In the framework of this study, we have demonstrated, that compound **1** selectively binds to the $(dA)_{20}$ oligomer, as indicated by pronounced changes in the absorption and fluorescence spectra. On the other hand, the binding of **1** to DNA in the cell nuclei of living or fixed HeLa cells was not confirmed with confocal microscopy. This observation might be explained by the lower permeability of the nuclear membranes towards compound **1**. None of the three investigated compounds showed *in vitro* cytotoxicity in the examined HT-29 and MDA-MB-231 cell lines, which might reflects their similar structure and cellular localization. Bioimaging experiments with confocal microscopy show a non-uniform cellular distribution of compound **1** in live and fixed HeLa cells. Compound **1** stains cell membranes and the cytoplasm but not nuclei. Competition experiments with mitochondria-sensitive probes suggest the mitochondria as target cellular organelles for **1**. Co-staining experiments with **1** and **2** in living cells supports co-localization of both compounds in the same lipid compartments. Independent from the confocal microscopy studies on **1**, HR-CS AAS measurements confirmed the cellular uptake of **3** into cancer cells. Due to their similar structures, and the same log$P_{o/w}$ values and based on the HR-CS AAS measurement results, it can be hypothesized that non-luminescent

metallocenes **2** and **3** show the same pattern of cellular biodistribution as luminescent compound **1**. Thus, compound **1** can be regarded as a metal-free luminescent probe for the non-direct bioimaging of metallocenes **2** and **3** in live and fixed cells. Furthermore our work demonstrates in a broader context a high potential of [2.2]-paracyclophane derivatives as non-redox active analogs of bioactive compounds based on ferrocene.

Experimental Section

General Comments: All preparations were carried out using standard Schlenk techniques. Chromatographic separations were carried out using silica gel 60 (Merck, 230-400 mesh ASTM). DMF was distilled prior to use. Other solvents were of reagent grade and were used without prior purification. All other chemicals were purchased from the Aldrich Chemical Co. The NMR spectra were recorded on a Bruker AV600 Kryo (600 MHz) spectrometer. Chemical shifts are reported in δ (ppm) using residual DMSO (^{1}H δ 2.50 ppm, ^{13}C δ 39.70 ppm) as the reference. Mass spectra were recorded using ES methods on a Varian 500-MS iT mass spectrometer. IR spectra were recorded on an FTIR Nexus Nicolet apparatus. Microanalyses were performed by the Analytical Services of the Polish Academy of the Sciences (Łódź).

Synthesis of 3-chloropropionyl-[2.2]-paracyclophane 7: [2.2]-Paracyclophane (104 mg, 0.5 mmol) dissolved in dichloromethane (10 ml) was treated with 3-chloropropionylchloride (100 µl, 1.0 mmol) and $AlCl_3$ (120 mg, 0.9 mmol) at -50°C. After 20 min stirring at -20°C, the reaction mixture was poured onto 5% aqueous HCl solution, extracted with diethyl ether, washed with aqueous Na_2CO_3, dried over $MgSO_4$ and evaporated to dryness. The residue was subjected to column chromatography on SiO_2 (eluent: CH_2Cl_2/*n*-hexane, 1:1). Crystallization from CH_2Cl_2/*n*-hexane gave pure **7** (yellowish solid) in 53% (79 mg) yield. ^{1}H NMR (400 MHz, DMSO-d_6): δ = 7.09(d, $J_{H,H}$ = 1.7 Hz, 1H, paracyclophane), 6.73(dd, $J_{H,H}$ = 7.7 Hz, 1.7 Hz, 1H, paracyclophane), 6.58(d, $J_{H,H}$ = 7.7 Hz, 1H, paracyclophane), 6.55(dd, $J_{H,H}$ = 7.8 Hz, 1.7 Hz, 1H, paracyclophane), 6.51(dd, $J_{H,H}$ = 7.8 Hz, 1.7 Hz, 1H, paracyclophane), 6.44(dd, $J_{H,H}$ = 7.8 Hz, 1.8 Hz, 1H, paracyclophane), 6.37(dd, $J_{H,H}$ = 7.8 Hz, 1.8 Hz, 1H, paracyclophane), 3.93(m, 2H, CH_2), 3.83(m, 1H, CH_2), 3.49(m, 1H, CH_2), 3.22(m, 1H, CH_2), 3.06(m, 6H, CH_2), 2.84(m, 1H, CH_2). ^{13}C{^{1}H} NMR (150 MHz, DMSO-d_6): δ = 198.4, 140.9, 140.0, 139.5, 139.3, 137.1, 136.6, 136.3, 133.9, 133.1, 132.8, 132.1, 131.1, 42.2, 40.0, 35.2, 34.6, 34.5, 34.4. MS (EI, 70 eV): m/z = 263 (M^+-Cl). FTIR (KBr): 3007, 2962, 2926, 2855, 1676(C=O), 1606(C=O), 1509, 1414, 1351,1236, 1181, 829,569 cm^{-1}. Anal. Calcd for $C_{19}H_{19}ClO$: C, 76.37; H, 6.41. Found: C, 76.35; H, 6.47%.

Synthesis of compound 4: To a stirred solution of **7** (149 mg, 0.5 mmol) in DMF (10 ml) at room temperature was added 153 µl (1.1 mmol) of trimethylamine. After stirring for 20 minutes, 5-iodouracil (142 mg, 0.6 mmol) was added in ~4 ml of DMF, and the mixture was stirred at a 70°C for 5 h. Subsequently, the solvent was evaporated, and the residue was subjected to column chromatography on SiO_2 (eluent: CH_2Cl_2/methanol, 50:0.5). Crystallization from dichloromethane/*n*-hexane gave pure **4** (yellowish solid) in 76% (190 mg) yield. ^{1}H NMR (400 MHz, DMSO-d_6): δ = 11.69 (s, 1H, H-N), 8.28(s, 1H, uracil), 7.07(s, 1H, paracyclophane), 6.72(d, $J_{H,H}$ = 9.8 Hz, 1H, paracyclophane), 6.52(m, 3H, paracyclophane), 6.39(d, $J_{H,H}$ = 9.9 Hz, 1H, paracyclophane), 6.25(d, $J_{H,H}$ = 9.9 Hz, 1H, paracyclophane), 4.10-3.78(m, 2H, CH_2), 3.13-2.84(m, 10H, CH_2). ^{13}C{^{1}H} NMR (150 MHz, DMSO-d_6): δ = 161.1, 150.7, 150.6, 140.9, 139.9, 139.4, 139.3, 137.1, 136.6, 136.3, 134.1, 133.2, 132.8, 132.0, 130.9, 67.7, 44.2, 38.4, 35.2, 34.6, 34.4, 34.4. MS (EI, 70 eV): m/z = 238 (iodouracil). FTIR (KBr): 3053, 2926, 2853, 1683(C=O), 1608(C=O), 1439, 1220 cm^{-1}. Anal. Calcd for $C_{23}H_{21}N_2O_3I$: C, 55.21; H, 4.23. Found: C, 55.49; H, 4.51%.

General procedure for the synthesis of compounds 1-3: A Deoxygenated mixture of 5-iodouracil derivative **4** (250 mg, 0.5 mmol), **5** (239 mg, 0.5 mmol), or **6** (262 mg, 0.5 mmol), 1-ethynylpyrene (339 mg, 1.5 mmol), trimethylamine (139 µl, 1.0 mmol), DMF (10 ml), copper (I) iodide (190 mg, 1.0 mmol), triphenylphosphine (13 mg, 0.05 mmol), and tetrakis(triphenylphosphine)palladium (0) (58 mg, 0.05 mmol) was stirred at 30°C for 1.5 h. Then, the reaction mixture was evaporated to dryness. The residue was subjected to column chromatography on SiO_2 (eluent: CH_2Cl_2/methanol, 50:0.5). Crystallization from CH_2Cl_2/*n*-hexane afforded pure compound **1** (52%, 155 mg, yellow solid), **2** (56%, 162 mg, red-orange solid), or **3** (55%, 172 mg, yellow solid). **1**: ^{1}H NMR (600 MHz, DMSO-d_6): δ = 11.78 (s, 1H, H-N), 8.66 (d, $J_{H,H}$ = 9.0 Hz, 1H, pyrene), 8.50 (s, 1H, uracil), 8.37(m, 2H, pyrene) 8.35(d, $J_{H,H}$ = 9.0 Hz, 1H, pyrene), 8.30(d, $J_{H,H}$ = 7.8 Hz, 1H, pyrene), 8.25(d, $J_{H,H}$ = 8.9 Hz, 1H, pyrene), 8.21(d, $J_{H,H}$ = 8.9 Hz, 1H, pyrene), 8.17(d, $J_{H,H}$ = 7.9 Hz, 1H, pyrene), 8.13(t, $J_{H,H}$ = 7.6 Hz, 1H, pyrene), 7.13(s, 1H, paracyclophane), 6.73(d, $J_{H,H}$ = 7.6 Hz, 1H, paracyclophane), 6.59(d, $J_{H,H}$ = 7.7 Hz, 1H, paracyclophane), 6.55(d, $J_{H,H}$ = 7.9 Hz, 1H, paracyclophane), 6.50(d, $J_{H,H}$ = 7.9 Hz, 1H, paracyclophane), 6.46(dd, $J_{H,H}$ = 7.7 Hz, 1.2 Hz, 1H, paracyclophane), 6.34(dd, $J_{H,H}$ = 7.7 Hz, 1.2 Hz, 1H, paracyclophane), 4.20(m, 1H, CH_2), 4.10(m, 1H, CH_2), 3.88(pt, 1H, $J_{H,H}$ = 11.0 Hz, 1H, CH_2), 3.54(m, 1H, CH_2), 3.24(m, 1H, CH_2), 3.03(m, 6H, CH_2), 2.85(m, 1H, CH_2). ^{13}C{^{1}H} NMR (150 MHz, DMSO-d_6): δ = 199.8, 162.2, 150.1, 149.7, 140.9, 140.0, 139.4, 139.3, 137.1, 136.7, 136.3, 134.2, 133.2, 132,88, 132.0, 131.0, 131.0, 130.9, 130.8, 130.6, 129.0, 128.7, 128.3, 127.3, 126.8, 126.0, 125.9, 125.0, 123.8, 123.5, 117.1, 97.5, 91.2, 88.5, 44.7, 38.5, 35.3, 34.6, 34.4. MS (EI, 70 eV): m/z = 336 (M^+-acryloyl[2.2]paracyclophane), 262 (acryloyl[2.2]paracyclophane). FTIR (KBr): 3044, 2926, 2852, 2211(C≡C), 1697(C=O), 1626(C=O), 1453, 1337, 848 cm^{-1}. Anal. Calcd for $C_{41}H_{30}N_2O_3$: C, 82.25; H, 5.05. Found: C, 82.31; H, 5.17%.

2: ^{1}H NMR (600 MHz, DMSO-d_6): δ = 11.79(s, 1H, H-N), 8.67(d, $J_{H,H}$ = 9.1 Hz, 1H, pyrene), 8.47(s, 1H, uracil), 8.37(m, 2H, pyrene) 8.35(d, $J_{H,H}$ = 9.1 Hz, 1H, pyrene), 8.31(d, $J_{H,H}$ = 8.0 Hz, 1H, pyrene), 8.26(d, $J_{H,H}$ = 8.9 Hz, 1H, pyrene), 8.22(d, $J_{H,H}$ = 8.9 Hz, 1H, pyrene), 8.18(d, $J_{H,H}$ = 7.9 Hz, 1H, pyrene), 8.13(t, $J_{H,H}$ = 7.5 Hz, 1H, pyrene), 4.86(pt, $J_{H,H}$ = 1.9 Hz, 2H, Cp'), 4.61(pt, $J_{H,H}$ = 1.9 Hz, 2H, Cp'), 4.25(s, 5H, Cp), 4.12(t, $J_{H,H}$ = 6.8 Hz, 2H, CH_2), 3.30(t, $J_{H,H}$ = 6.8 Hz, 2H, CH_2 overlapped with H_2O signal in DMSO-d_6). ^{13}C{^{1}H} NMR (150 MHz, DMSO-d_6): δ = 201.4, 162.2, 150.1, 149.9, 131.0, 130.9, 130.8, 130.6, 129.0, 128.7, 128.3, 127.3, 126.8, 126.07, 126.0, 125.1, 125.0, 123.8, 123.5, 117.1, 97.3, 91.3, 88.6, 78.6, 72.5, 69.8, 69.2, 44.6, 37.5. MS (EI, 70 eV): m/z = 336 (M^+-acryloylferrocene), 240 (acryloylferrocene). FTIR (KBr): 3169, 3037, 2918, 2216(C≡C), 1726(C=O), 1673(C=O), 1655(C=O), 1457, 1369, 1284, 850, 495 cm^{-1}. Anal. Calcd for $C_{35}H_{24}N_2O_3Fe$: C, 72.93; H, 4.20. Found: C, 72.78; H, 4.50%.

3: ^{1}H NMR (600 MHz, DMSO-d_6): δ = 11.78 (s, 1H, H-N), 8.66 (d, $J_{H,H}$ = 9.1 Hz, 1H, pyrene), 8.40 (s, 1H, uracil), 8.37(m, 2H, pyrene) 8.35(d, $J_{H,H}$ = 9.1 Hz, 1H, pyrene), 8.31(d, $J_{H,H}$ = 8.0 Hz, 1H, pyrene), 8.26(d, $J_{H,H}$ = 8.9 Hz, 1H, pyrene), 8.21(d, $J_{H,H}$ = 8.9 Hz, 1H, pyrene), 8.17(d, $J_{H,H}$ = 7.9 Hz, 1H, pyrene), 8.13(t, $J_{H,H}$ = 7.6 Hz, 1H, pyrene), 5.17(pt, $J_{H,H}$ = 1.8 Hz, 2H, Cp'), 4.87(pt, $J_{H,H}$ = 1.8 Hz, 2H, Cp'), 4.04(s, 5H, Cp), 4.05(t, $J_{H,H}$ = 6.7 Hz, 2H, CH_2), 3.16(t, $J_{H,H}$ = 6.7 Hz, 2H, CH_2). ^{13}C{^{1}H} NMR (150 MHz, DMSO-d_6): δ = 199.1, 162.2, 150.0, 149.8, 131.0, 130.9, 130.8, 130.6, 129.0, 128.7, 128.3, 127.3, 126.8, 126.0, 125.9, 125.1, 125.0, 123.8, 123.5, 117.1, 97.3, 91.3, 88.5, 83.5, 73.9, 72.0, 70.7, 44.7, 36.8. MS (EI, 70 eV): m/z = 336 (M^+-acryloylruthenocene), 286 (acryloylruthenocene). FTIR (KBr): 3193, 3043, 2960, 2214(C≡C), 1728(C=O), 1676(C=O), 1655(C=O), 1458, 1375, 1283, 848 cm^{-1} . Anal. Calcd for $C_{35}H_{24}N_2O_3Ru$: C, 67.62; H, 3.89. Found: C, 67.73; H, 3.77%.

Electronic absorption and emission properties of 1: UV-Vis absorption spectra were recorded with a Varian Cary 300 double beam spectrometer, and luminescence spectra were measured with a Horiba Jobin Yvon Fluorolog 3 steady-state fluorescence spectrometer. Photoluminescence quantum yields were determined with a Hamamatsu

C9920-02 system. For decay time measurements, the emission was excited with pulsed laser irradiation (pulse duration of approximately 80 fs, excitation wavelength 370 nm) generated using a Ti-sapphire pumping laser (Libra Coherent) and a TOPAS-C (Light Conversion) optical parametric amplifier. The emission was detected by a Bruker 200is spectrograph connected to a Hamamatsu C7700 streak camera. The streak images were recorded on a Hamamatsu (ORCA-CR) CCD camera. For each sample, a total of 8000 excitation shots were applied. The decay times were obtained from a global analysis of the collected time-resolved data.

Molecular structure and TD-DFT calculations: Quantum mechanical computations were performed using the NWChem computer program.[24] For numerical data analysis, the Chemissian program was used.[25] The ground state geometry and TD-DFT electronic transitions were computed using the B3LYP functional[26] and the Ahlrichs def2-svp basis set[27] for all atoms.

Interaction of 1 with oligonucleotide $(dA)_{20}$: We used water from a Milli-Q system with a resistivity of 18.2 MΩ·cm. DMSO p.a. was purchased from *Carl Roth*, and oligonucleotides were purchased from *Metabion*. Absorption spectra were recorded on a *Varian Cary 100* spectrometer equipped with a 6x6 cell changer unit. The samples were recorded in water, DMSO or water + 0.6% DMSO using quartz glass cuvettes (10 mm). Emission spectra were measured on a *Jobin–Yvon FluoroMax 3* fluorimeter with a step width of 1 nm, an integration time of 0.2 s and an excitation and emission band pass of 2 nm. All spectra were recorded at 20 °C and corrected by a reference.

Confocal Microscopy: The cells were grown in Dulbecco's minimal essential medium (DMEM) with 5% (HeLa) or 10% (3T3) FCS, at 5% CO_2 and 37°C. The microscopy imaging and staining with organic fluorophores was performed in the same medium unless otherwise stated. The integrity of the plasma membranes was monitored using a propidium iodide (PI) exclusion test and a fluorescein diacetate (FDA) "vital" test, as described before.[28] Where indicated, the mitochondria of live cells were labelled with JC-1 (5,5′,6,6′-tetrachloro-1,1′,3,3′-tetraethylbenzimidazolylcarbocyanine) or TMRE (tetramethyl rhodamine, ethyl ester). The cells were incubated with 3 μM (JC-1) or 0.1 μM (TMRE) dye for 30 minutes. Alternatively, the cells were fixed in 5% formaldehyde (PBS) for 30 minutes and stained with acridine orange (AO, 10 μg/ml) in equilibrium conditions. The imaging was performed using an LSM 780 confocal system (Zeiss) equipped with an Axio Observer Z1 inverted microscope, 63× oil immersion objective (NA 1.4), 355 DPSS laser (20 mW), 488 nm Ar laser (25 mW) and 561 DPSS laser (20 mW) and a multi-anode PMT (32 elements). The luminescence spectrum was registered from single confocal sections (pinhole set to 1 Airy unit), in the 410 nm – 685 nm range, with 8.5 nm spectral precision. Where indicated, the detector elements were combined into detection bands corresponding to 410-470 nm (compound 1) and 570-630 nm (DsRed2). The luminescence and transmitted light images were collected with a 4.2 μs pixel dwell time and a pixel size of 0.118 μm. Luminescence lifetime was measured with SP8 confocal system (Leica) equipped with DMI 6000 inverted microscope, 63× oil immersion objective (NA 1.4), 405 nm pulsed laser (20 MHz). The luminescence (compound **1**) was registered in 460-550 nm band with SPAD detector operating in time-correlated single photon counting (TCSPC) mode. Laser power was adjusted so as to keep the average count rate at ~700 kcps.

Cytotoxicity and cellular ruthenium uptake. Cell culture: HT-29 colon and MCF-MB-231 breast carcinoma cells were maintained in Dulbecco's Modified Eagle Medium (4.5 g/L D-Glucose, L-Glutamine, Pyruvate), which was supplemented with gentamycin (50.0 mg/L) and foetal bovine serum superior, standardized (Biochrom GmbH, Berlin) (10% V/V), and were passaged once a week. **Cytotoxicity assay**: The antiproliferative effects were determined according to a recently used method with minor modifications.[29] In short: a volume of 100 μL of HT-29 cells (2565 cells/mL) or MDA-MB-231 (4120 cells/mL) was transferred into the wells of 96-well plates and incubated at 37 °C / 5% CO_2 for 72 h. Stock solutions of the compounds in DMF were freshly prepared and diluted with the respective cell culture medium to graded concentrations in the range of 0.2 – 100 μM (final DMF 0.1% v/v). After 72 h of exposure, the cell biomass was determined by crystal violet staining, and the IC50 value was determined as the concentration that caused 50% inhibition of cell proliferation compared to an untreated control. The results were calculated as the mean of two independent experiments.

Cellular Uptake Studies in HT-29 Cells: The cellular metal uptake was determined according to previously described methods.[30] In short: HT-29 colon carcinoma cells were grown until at least 75-80% confluency in 75 cm^2 cell-culture flasks. Stock solutions of the compounds in DMF were prepared and diluted with cell-culture medium to a final concentration of 5.0 μM immediately before use (final DMF concentration: 0.1% v/v). The cell culture medium of the flasks was replaced with medium containing the metal compound (10 mL), and the flasks were incubated at 37 °C / 5% CO_2 up to 6 h. After the desired incubation period, the uptake was stopped by removing the cell culture medium. The cells were washed with PBS (10 mL), the washing solution was removed, and the cells were isolated after 3 min trypsinization (2.0 mL trypsin solution 0.05 %, containing EDTA 0.004%) by centrifugation. The obtained cell pellets were stored at –20 °C for further use. For metal and protein quantification, the pellets were resuspended in demineralized water (0.5 mL) and lysed for 30 min by ultra-sonication. The protein content of the lysates was determined by the Bradford method, and the metal content was determined by AAS, as described below.

HR-CS AAS measurements: For the ruthenium measurements, a contrAA 700 high-resolution continuum-source atomic absorption spectrometer (Analytik Jena AG) was used. Pure samples of the respective complexes were used as standards, and calibration was conducted in a matrix-matched manner (standards were prepared using blank cellular lysates; samples and standards were adjusted to the same cell protein concentration by dilution with distilled water). Triton-X 100 (1%, 10 μL) and nitric acid (13%, 10 μL) were added to each standard and sample (100 μL). Probes were injected (25 μL) into coated standard graphite tubes (Analytik Jena AG) and thermally processed as previously described with minor modifications (see oven program in Table S3 (*Supplementary Information*).[30] Ruthenium was quantified at a wavelength of 349.90 nm. The mean integrated absorbance of triple injections was used throughout the studies. The final results were calculated from data obtained in two independent experiments and are expressed as nmol of metal per mg of cellular protein.

HPLC: The analytes were separated by an Agilent 1200 system (Agilent Technologies, USA) equipped with DAD on a Zorbax Eclipse XBD column (C18, 250 x 4.6 mm ID, Agilent Technologies, USA). The separation was isocratic, using as a mobile phase water-methanol (HPLC gradient grade, Sigma-Aldrich) mixtures containing 0.7, 0.75, 0.8, 0.85, 0.9 and 0.95 volume fractions of organic modifier. The flow rate was 1.5 mL/min. The tested compounds were detected under UV light at 230 nm. All measurements were conducted at 20°C. The dead time values were measured from the peaks of the effluents. All runs were performed in triplicate, and the resulting average values were used for the calculation of the retention factors. The system was connected to a computer with the software ChemStation Data Analysis, enabling the operation and maintenance of all subsystems of the apparatus for HPLC, registration and analysis of the measurement results.

Acknowledgements

J.S. thanks the National Science Centre in Cracow, Poland (Grant Preludium no. DEC-2012/05/N/ST5/01055) for financial support. H-A.W. and P.E. thank the Karlsruhe School of Optics and Photonics (KSOP). RC thanks for funding from the European Union's Horizon 2020 research and innovation programme under the Marie Skłodowska-Curie grant agreement No. 645628.

Keywords: ferrocene / ruthenocene / [2.2]-paracyclophane / bioimaging / bioorganometallics

References

[1] B. Lippert, *Cisplatin: Chemistry and Biochemistry of a Leading Anticancer Drug*, Wiley, New York, **1999**.

[2] a) G. Jaouen, M. Salmain, *Bioorganometallic Chemistry: Applications in Drug Discovery, Biocatalysis, and Imaging*, John Wiley & Sons, UK, **2015**; b) D. R. Van Staveren, N. Metzler-Nolte, Chem. Rev. **2004**, *104*, 5931-5985; c) N. Metzler-Nolte, M. Salmain, *Ferrocenes: Ligands, Materials and Biomolecules, Chapter 13* (Ed.: P. Štěpnička), John Wiley & Sons, UK, **2008**, pp. 499-639; d) C. G. Hartinger, P. J. Dyson, *J. Chem. Soc. Rev.* **2009**, *38*, 391-402; e) G. Jaouen, N. Metzler-Nolte, *Medicinal Organometallic Chemistry in a series Topics in Organometallic Chemistry*, Vol. 32, Springer, **2010**; f) M. Patra, G. Gasser, N. Metzler-Nolte, *Dalton. Trans.* **2012**, *41*, 6350-6358; g) M. Patra, G. Gasser, *ChemBioChem.* **2012**, *13*, 1232-1252; h) K. Heinze, H. Lang, *Organometallics* **2013**, *32*, 5623-5625; i) I. Ott, Coord. *Chem. Rev.* **2009**, *253*, 1670-1681; j) F. Hackenberg, M. Tacke, *Dalton Trans.* **2014**, *43*, 8144-8153; k) J. É. Debreczeni, et al. *Chem., Int. Ed.* **2006**, *45*, 1580-1585; l) B. S. Murray, et al. *Coord. Chem. Rev.* **2016**, *306*, 86-114; m) C. R. Munteanu, K. Suntharalingam, *Dalton Trans.* **2015**, *44*, 13796-13808.

[3] a) C. Ornelas, *New J. Chem.* **2011**, *35*, 1973-1985; b) G. Jaouen, A. Vessières, S. Top, *Chem. Soc. Rev.* **2015**, *44*, 8802-8817.

[4] a) C. Biot, et al. *J. Med. Chem.* **1997**, *40*, 3715-3718; b) L. Delhaes, et al. *ChemBioChem* **2002**, *3*, 418-423; c) F. Dubar, et al. *Chem. Commun.* **2012**, *48*, 910-912.

[5] a) T. J. Kealy, P. Pauson, *Nature* **1951**, *168*, 1039-1040; b) S. A. Miller, J. A. Tebboth, J. F. Tremaine, *J. Chem. Soc. Rev.* **1952**, 632-635; c) R. B. Woodward, M. Rosenblum, M. C. Whiting, *J. Am. Chem. Soc.* **1952**, *74*, 3458-3459; d) J. D. Dunitz, L. E. Orgel, *Nature* **1953**, *171*, 121-122; e) P. Seller, J. D. Dunitz, *Acta Crystallogr. Sect. B* **1979**, *35*, 2020-2032; f) N. Long, *Metallocenes-An Introduction to Sandwich Complexes* Blackwell Science, Oxford, **1998**; g) R. D. Adams, *J. Organomet. Chem.* **2001**, *637-639*, 1-69; h) P. Štěpnička (Ed.), *Ferrocenes: Ligands, Materials and Biomolecules*, John Wiley & Sons, Ltd, UK, **2008**; i) A. Togni, T. Hayashi (Eds.), *Ferrocenes: Homogeneous Catalysis, Organic Synthesis, Materials Science*, John Wiley & Sons, Ltd, Weinheim, Germany, **1995**.

[6] a) E. Baggaley, J. A. Weinstein, J. G. Williams, *Coord. Chem. Rev.* **2012**, *256*, 1762-1785; b) S. Kaloyanova, et al. *J. Am. Chem. Soc.* **2016**, *138*, 2881-2884; c) K. K-W. Lo, Acc. *Chem. Res.* **2015**, *48*, 2985-2995; d) C. D. Geddes, J. R. Lakowicz, *Topics in Fluorescence Sensing*, Vol. 10. Springer-Verlag, New York, USA, **2005**; e) B. Herman, *Fluorescence Microscopy*, Springer-Verlag, New York, USA, **1998**; f) S. Chen, et al. *Analyst* **2010**, *135*, 577-582.

[7] S. I. Kirin, et al. *Angew. Chem. Int. Ed.* **2008**, *47*, 955-959.

[8] A. R. Ghezzi, et al. *J. Inorg. Biochem.* **2004**, *98*, 73-78.

[9] R. A. Alderden, et al. *J. Am. Chem. Soc.* **2007**, *129*, 13400-13401.

[10] a) C. Policar, et al. *Angewandte Chemie* (International ed. in English) **2011**, *50*, 860-864; b) K. Meister, et al. *Angewandte Chemie* (International ed. in English) **2010**, *49*, 3310-3312; c) K. V. Kong, et al. *Bioconjugate Chem.* **2007**, *18*, 1370-1374; d) K. V. Kong, et al. *Olivo, Angewandte Chemie* (International ed. in English) **2012**, *51*, 9796-9799.

[11] S. Clède, C. Policar, *Chem. Eur. J.* **2014**, *21*, 942-958.

[12] a) C. J. Brown, A. C. Farthing, *Nature* **1949**, *164*, 915-916; b) D. J. Cram, H. Steinberg, *J. Am. Chem. Soc*. **1951**, *73*, 5691-5704; c) D. J. cram, J. M. Cram, *Acc. Chem. Res.* **1971**, *4*, 204-213; d) T. Sato, K. Torizuka, *J. Chem. Soc. Perkin Trans.* **1978**, *2*, 1199-1204.

[13] K. A. Lyssenko, M. Y. Antipin, D. Y. Antonov, *ChemPhysChem* **2003**, *4*, 817-823.

[14] a) Leo, C. Hansch, D. Elkins, *Chem. Rev.* **1971**, *71*, 525-616; b) R. Ahmedi, T. Lanez, *J. Fundam. Appl. Sci.* **2011**, *3*, 183-193.

[15] a) K. Schlotter, et al. *J. Med. Chem.* **2006**, *49*, 3628-3635; b) K. Schlotter, et al. *J. Med. Chem.* **2005**, *48*, 3696-3699.

[16] a) K. Kowalski, et al. *Organometallics* **2013**, *32*, 5766-5773; b) J. Skiba, et al. *J. Organomet. Chem.* **2015**, *782*, 52-61; c) H. V. Nguyen, et al. *J. Med. Chem.* **2014**, *57*, 5817-5822; d) M. Hocek, et al. *Chem. Eur. J.* **2004**, *10*, 2058-2066; e) P. James, et al. *Org. Lett.* **2006**, *8*, 2763-2766; f) H. V. Nguyen, et al. *Organometallics* **2011**, *30*, 5284-5290; g) K. Kowalski, *Coord. Chem. Rev.* **2016**, *317*, 132-156.

[17] a) P. Ensslen, Y. Fritz, H.-A. Wagenknecht, *Org. Biomol. Chem.* **2015**, *13*, 487-492; b) J. Barbaric, H.-A. Wagenknecht, *Org. Biomol. Chem.* **2006**, *4*, 2088-2090; c) V. Astakhova, D. Lindegaard, V. A. Korshun, *J. Wengel, Chem. Commun.* **2010**, *46*, 8362; d) J. B. Birks, L. G. Christophorou, *Spectrochim. Acta* **1963**, *19*, 401-410; e) N. Turro, V. Ramamurthy, J. C. Scaiano, *Modern Molecular Photochemistry of Organic Molecules,* University Science Books, Sausalito, USA, **2010**, p. 253 and p. 961; f) J. R. Lakowicz, *Principles of Fluorescence Spectroscopy, 3rd ed.* Baltimore, USA, **2006**; g) B. Juskowiak, *Anal. Bioanal. Chem*. **2011**, *399*, 3157–3176.

[18] I. Ott, C. Biot, C. Hartinger in *Inorganic Chemical Biology: Principles, Techniques and Applications*, (Ed.: G. Gasser) John Wiley & Sons, Ltd, UK, **2014**.

[19] G. Crawford, et al. *J. Am. Chem. Soc.* **2011**, *133*, 13349–13362.

[20] K. Kalyanasundaram, J. K. Thomas, *J. Am. Chem. Soc.* **1977**, *99*, 2039-2044.

[21] S. Sezi, H.-A. Wagenknecht, *Chem. Commun*. **2013**, *49*, 9257-9259.

[22] a) European Commission, *Official Journal of the European Union* **2008**, *440*, 67-74; b) OECD, *Test No. 117: Partition Coefficient (n-octanol/water), HPLC Method*, *OECD Guidelines for the Testing of Chemicals, Section 1*, OECD Publishing, Paris, **2004**; c) C. V. Eadsforth, P. Moser, *Chemosphere* **1983**, *12*, 1459-1475; d) E. Soczewiński, C. A. Wachtmeister, *J Chromatogr.* **1962**, *7*, 311–317.

[23] V. Rudraraju, et al. *Pharmazie,* **2014**, *69*, 655-662.

[24] M. Valiev, et al. *Comput. Phys. Commun.* **2010**, *181*, 1477-1489.

[25] L. Skripnikov, *Chemissian v. 4.33*, www.chemissian.com.

[26] a) D. Becke, *J. Chem. Phys*. **1993**, *98*, 5648-5652; b) P. J. Stephens, et al. *J. Phys. Chem.* **1994**, *98*, 11623-11627.

[27] F. Weigend, R. Ahlrichs, *Phys. Chem. Chem. Phys.* 2005, 7, 3297-3305.

[28] T. Bernaś, J. W. Dobrucki, *Micr. Res. Tech.* **2004**, *64*, 126-134.

[29] I. Ott, H. Scheffler, R. Gust, *ChemMedChem.* **2007**, *2*, 702-707.

[30] S. Schäfer, et al. *Eur. J. Inorg. Chem.* **2007**, *2007*, 3034-3046.

Table of Contents
Entry for the Table of Contents (Please choose one layout)

Layout 1:

FULL PAPER

Biodistribution of ferrocenyl and ruthenocenyl uracil-pyrenes in living and fixed cells is investigated *via* non-direct approach exploiting structural similarities of metallocenyl and [2.2]-paracyclophanyl group. Confocal microscopy studies on luminescent [2.2]-paracyclophane uracil-pyrene show its accumulation in membranes, cytoplasm and mitochondria of assayed cells. A similar biodistribution pattern is postulated for the metallocenyl congeners.

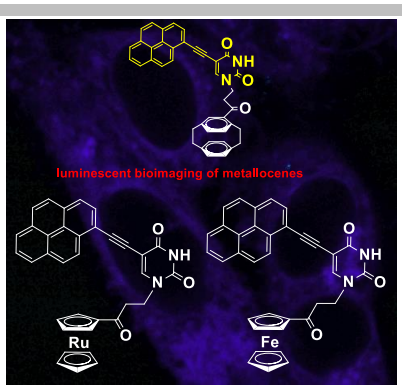

Bioimaging of metallocenes in living and fixed cells

*Author(s), Corresponding Author(s)**

Page No. – Page No.

Title

*one or two words that highlight the emphasis of the paper or the field of the study

Layout 2:

FULL PAPER

((Insert TOC Graphic here; max. width: 11.5 cm; max. height: 2.5 cm; NOTE: the final letter height should not be less than 2 mm.))

Key Topic*

*Author(s), Corresponding Author(s)**

Page No. – Page No.

Title

Text for Table of Contents

*one or two words that highlight the emphasis of the paper or the field of the study